

Protoplanetary disc population synthesis

I. Constraining disc parameters to reproduce disc observations

Jose. L. Gomez^{1,2}, Octavio. M. Guilera^{1,2}, Marcelo. M. Miller Bertolami^{1,2}, Elisa Castro-Martínez³ and María. Paula Ronco^{1,2}

¹ Instituto de Astrofísica de La Plata, CCT La Plata, CONICET-UNLP, Paseo del Bosque S/N, B1900FWA La Plata, Argentina

² Facultad de Ciencias Astronómicas y Geofísicas, UNLP, Paseo del Bosque S/N, B1900FWA La Plata, Argentina

³ University of Grenoble Alpes, CNRS, IPAG, 38000 Grenoble, France

e-mail: josepluis21@gmail.com

Received XX, 2025; accepted XX, 2025

ABSTRACT

Context. Protoplanetary discs are the birthplaces of planets. Recent studies highlight the importance of stellar mass sampling when determining disc lifetimes through the observed fraction of stars with discs. Low-mass stars tend to host discs with average lifetimes exceeding 5 Myr, providing sufficient time for planet formation via solid accretion. In addition, observations show a strong correlation between stellar (and substellar) mass and accretion rate, typically following the relation $\dot{M} \propto M^2$.

Aims. This study aims to identify the optimal parameters of a protoplanetary disc evolution model capable of reproducing both the observed disc fractions and the mass accretion rates in young stellar populations.

Methods. We conducted a population synthesis study where disk evolution was modeled exploring different values of the viscosity parameter α as a function of stellar mass. Disc evolution was modeled through viscous accretion and photoevaporation (internal and external). Initial disc masses and radii were drawn from observationally motivated statistical distributions. We also introduce on our population synthesis a stellar mass distribution and a star formation rate (SFR).

Results. Matching the observed disc fractions and accretion trends requires that the α -viscosity parameter increases with stellar mass. External photoevaporation is needed to generate low-mass discs with high accretion rates, while accounting for a time-dependent SFR enhances accretion in young clusters and extends disc lifetimes in older ones. In addition, introducing a stellar mass cut-off reproduces the distance-dependent biases seen in cluster disc fractions.

Conclusions. Our results indicate that both stellar and environmental dependencies are essential to explain the observed properties of protoplanetary discs. A stellar-mass-dependent viscosity is required to recover the $\dot{M}-M_\star$ relation, while external photoevaporation and extended star formation histories shape the distribution of accretion rates across different environments. These findings highlight the need for multi-faceted population synthesis models to connect disc evolution with planet formation pathways.

Key words. Protoplanetary discs – accretion discs – methods: numerical

1. Introduction

Recent studies have provided large samples of young stellar objects confirmed in star-forming regions and young stellar associations (e.g. Manara et al. 2016; Tazzari et al. 2017; Manara et al. 2023). These comprehensive datasets enable robust estimates of the fraction of stars with protoplanetary discs, which in turn allow for more precise determinations of disc dispersal timescales. Throughout the lifetime of a protoplanetary disc, both its gas and dust components undergo significant evolution. During this phase, planet formation occurs (e.g. Armitage 2009), followed by planet–disc interactions that play a key role in driving planetary migration (e.g. Venturini et al. 2020b; Drazkowska et al. 2022). The disc lifetime is thus a fundamental parameter that governs the architecture of emerging planetary systems.

Variations in the morphology and evolution of key disc parameters are driven by physical processes that are critical for understanding the formation and evolution of planets and planetary systems. The wide diversity observed in planetary populations may largely be explained by the complex interplay of these disc

evolutionary processes. Gaining insight into this evolution is essential to identify the conditions under which planet formation occurs. Accurate modeling of protoplanetary discs is therefore a fundamental step toward a comprehensive understanding of planet formation.

Early studies of protoplanetary disc lifetimes suggested that discs typically disperse within 1 to 10 Myr, with an average lifetime of approximately 3 Myr (e.g. Haisch Jr et al. 2001; Majajek 2009; Pfalzner et al. 2014). However, more recent analyses indicate that disc lifetimes may be significantly longer. Pfalzner et al. (2022) highlight that observational samples of clusters are often biased by magnitude limits, resulting in an over-representation of high-mass stars in disc fraction estimates. Since protoplanetary discs around intermediate and massive stars evolve and dissipate faster (e.g. Ribas et al. 2015; Kunitomo et al. 2021; Ronco et al. 2024), this bias leads to a systematic underestimation of disc lifetimes. When accounting for stellar mass and distance biases, disc lifetimes appear to span a broader range, from 1 to 20 Myr, with most discs around low-mass stars persisting beyond 5 Myr (Pfalzner et al. 2022; Pfalzner & Dincer 2024).

Send offprint requests to: Jose L. Gomez

Disc dissipation timescales are strongly influenced by mass-loss processes, primarily viscous accretion onto the central star and photoevaporation driven by stellar radiation –both from the host star and from nearby massive stars. As a result, the evolution of protoplanetary discs depends on intrinsic disc properties, stellar characteristics, and the surrounding environment in which the discs reside (e.g. Coleman & Haworth 2022).

The long-term evolution of protoplanetary disks is currently modeled by two main theoretical frameworks: the viscous accretion disc model (e.g. Lynden-Bell & Pringle 1974; Pringle 1981), and the model of magnetically driven disc winds (e.g. Blandford & Payne 1982; Suzuki & Inutsuka 2009). A major challenge in current research is validate these models through observational constraints. However, tracking the full evolutionary path of an individual disc is not possible. Therefore, testing theoretical models requires statistical analyses of large disc populations, rather than case-by-case comparisons.

In recent years, several models have been developed to reproduce the observed properties of protoplanetary disc populations using simplified physical prescriptions. Coleman & Haworth (2022) demonstrated that ongoing star formation is necessary to match the observed disc fractions as a function of cluster age. Their results also highlight the importance of including both internal and external photoevaporative winds to accurately describe disc evolution. In environments with high ultraviolet radiation fields, transition discs are predicted to be rare –a trend that is consistent with their observed spatial distribution in the Orion Nebula Cluster.

Efforts to refine the initial conditions that best reproduce disc observations have been explored by Emsenhuber et al. (2023), who found that disc lifetimes are too short when both internal and external photoevaporation are included simultaneously. A better match to the disc properties in the Lupus and Chamaeleon I low-mass star-forming regions was achieved by assuming initially more massive, compact discs subject only to internal photoevaporation.

The objective of this study is to reproduce the main observational features of protoplanetary discs through a population synthesis framework in which discs evolve under viscous accretion and both internal and external photoevaporation. We restrict our analysis to the gaseous component of the discs, adopting initial conditions derived from observations of Class 0/I star-forming regions and complemented by theoretical and experimental constraints. Particular attention is given to the role of observational biases: we assess the impact of magnitude limits, which vary with distance, on the inferred fraction of stars with discs by applying different stellar mass cut-offs. Furthermore, since star formation in young clusters does not occur simultaneously, we also investigate the influence of a time-dependent star formation rate on the resulting disc fractions as a function of cluster age and on the distribution of stellar accretion rates. A summary of our main findings is presented in the main text, with a more detailed analysis provided in the appendices.

The paper is structured as follows: in Sec. 2 we present the method for performing the population synthesis and we describe the model used to compute the disc evolution. In Sec 3 we present the observational constraints for our population synthesis results. We then present the results of our study in Sec. 4, focusing on finding the best initial condition for the population, exploring how the α correlation with stellar masses and the SFR affect the lifetime and mass accretion rate. This is followed by a discussion of our results in Sec 5. Finally, we present our conclusions in Sec 6.

2. Population synthesis model

The modeling of the whole population of protoplanetary discs in a given young stellar population requires many different physical ingredients. First of all we need to know the distribution of stellar masses resulting from the fragmentation of the original molecular cloud. Then, we need to know how the masses and radii of the discs correlate with the mass of the central stars. Moreover, in order to predict the properties of protoplanetary discs at a given time we need to know the age of each individual disc, and how do they change with time. Some of these properties are relatively well understood, and similar in all populations, and can be statistically derived from observations. Conversely, other parameters of the model will depend both on the specific details of a given stellar population and/or will depend on the underlying physical model of the disc, and need to be calibrated to reproduce specific populations. Below we describe how different ingredients have been adopted in our current population synthesis model. For each choice of the physical parameters of each population, 10000 random star-disc systems were simulated to derive the underlying statistical distributions.

2.1. Initial stellar mass function

The initial stellar mass function implemented in this work is the one derived by Kroupa (2001). The probability distribution of stellar masses (M_*) in each stellar population is given by:

$$\xi(M_*) \propto \begin{cases} M_*^{-0.3}, & 0.01M_\odot \leq M_* < 0.08M_\odot, \\ M_*^{-1.3}, & 0.08M_\odot \leq M_* < 0.50M_\odot, \\ M_*^{-2.3}, & 0.50M_\odot \leq M_* < 10.0M_\odot. \end{cases} \quad (1)$$

Where stellar masses in our simulations are taken in the range 0.04–1.4 M_\odot . We take the normalization constant in each mass range so that the resulting probability distribution is continuous.

2.2. Star formation rate

Following the work of Coleman & Haworth (2022) we consider a star formation rate (SFR) that initially remains constant for a million years (SFR_0), and then drops exponentially with a characteristic decay time t_d . The SFR is then assumed to be

$$SFR(t) \propto SFR_0 \times \begin{cases} 1 & t < 1 \text{ Myr}, \\ \exp\left[-\frac{(t-1 \text{ Myr})^2}{t_d^2}\right] & t \geq 1 \text{ Myr}. \end{cases} \quad (2)$$

The SFR represents a distribution of initial times at which the different star-disc systems are implanted in our population synthesis. The Fig. 1 shows the initial distribution time for our population considering $t_d = 1$ Myr. We discuss the effect of considering different SFRs in Sec. 4.3.1.

2.3. Initial disc mass

The mass of the disc is dominated by the mass of the gas, which is mostly composed by molecular hydrogen and helium. While it is not possible to determine the total disc masses directly from molecular hydrogen emission, the thermal emission of the dust particles can be measured relatively easily and the measured flux values can be converted into dust masses (Tychoniec et al. 2018; Manara et al. 2023). We follow Emsenhuber et al. (2021) which use the statistical distribution of gas disc masses inferred for protostars located in Perseus by Tychoniec et al. (2018). These authors convert the dust mass to gas mass using a typical gas-to-

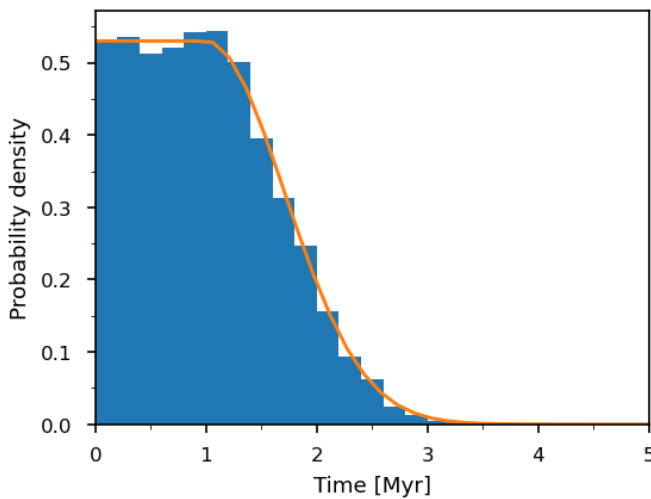


Fig. 1. The orange line represents the probability density of the star formation rate from Coleman & Haworth (2022). The blue histograms show the discrete probability apply for our population synthesis.

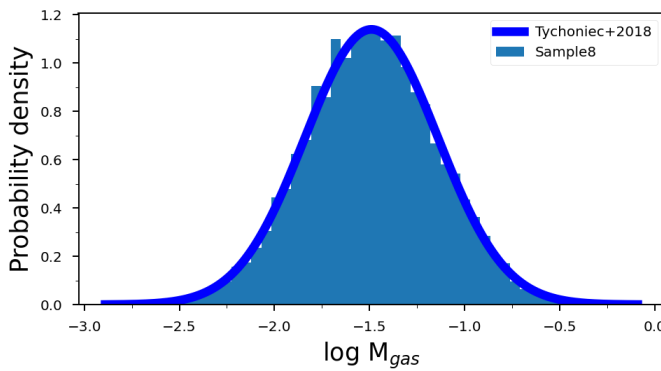


Fig. 2. The blue line represents the probability density of the disc masses (in term of the the mass of the host star) obtained by (Tychoniec et al. 2018). The dark blue histograms correspond to the disc mass sample for our population synthesis.

dust mass ratio of 100:1. This distribution represents a population of classes 0/I, shown in Fig. 2. The disc masses follow a log-normal probability distribution where the mean value is -1.49 and the dispersion is $\sigma = 0.35$. In this work, we consider a sample with a minimum limit of 3σ and a maximum limit of $0.2 M_\star$ to avoid possible disc gravitational instabilities.

2.4. Initial surface gas density

The initial surface density is chosen according to the work of Andrews et al. (2010), based on the similarity solutions given by Lynden-Bell & Pringle (1974) and Hartmann et al. (1998). Thus, the initial structure of the disc is represented by the following radial profile,

$$\Sigma_{\text{gas}} = \Sigma_{\text{gas}}^0 \left(\frac{R}{R_c} \right)^{-\gamma} e^{-(R/R_c)^{2-\gamma}}, \quad (3)$$

where Σ_{gas}^0 is a normalization constant related to the initial disc mass by

$$\Sigma_{\text{gas}}^0 = (2 - \gamma) \frac{M_{d,t=0}}{2\pi R_c^2}, \quad (4)$$

being R_c the characteristic radius of the disc, M_d is the initial mass of the disc and γ is the radial gradient which determines the initial mass distribution of the disc. For the surface density exponent we take the mean value obtained by Andrews et al. (2010), $\gamma = 0.9$, in all simulations.

For the characteristic radius R_c we follow Emsenhuber et al. (2021), who adopt the results from Andrews et al. (2010), and take R_c to be solely dependent on the mass of the disc,

$$\frac{R_c}{10 \text{ au}} = \left(\frac{M_d}{2 \times 10^{-3} M_\odot} \right)^{0.625}. \quad (5)$$

2.5. Disc evolution

Once the initial properties of the disc are decided, we need to model how different discs, around different stars, evolve with time. We compute the evolution of a circumstellar disc around a central star using the disc model implemented on PLANETALP (e.g Ronco et al. 2017; Guilera et al. 2017; Guilera et al. 2019). This model corresponds to an axi-symmetric 1D+1D, non-isothermal α -disc model. The assumption of an α -disc imples that the effective kinematic viscosity of the disc is given by $\nu = \alpha c_s H_g$ (Shakura & Sunyaev 1973), where H_g is the scale height of the disc, $H_g = c_s/\Omega$, where c_s is the local isothermal sound speed, and Ω is the keplerian-frequency. The material composing the gas disc is mainly molecular hydrogen and helium.

Within this framework the disc evolves by viscous accretion and photoevaporation, the latter both due to the irradiation from the central star and external sources (e.g. young massive stars in the population). The evolution of the surface density of the gaseous disc Σ_g follows a diffusion equation given by (Pringle 1981):

$$\frac{\partial \Sigma_g}{\partial t} = \frac{3}{R} \frac{\partial}{\partial R} \left[R^{1/2} \frac{\partial}{\partial R} (\nu R^{1/2} \Sigma_g) \right] + \dot{\Sigma}_w, \quad (6)$$

where $\dot{\Sigma}_w$ represents the sink term due to photoevaporation (e.g Guilera et al. 2017). The time evolution of the surface density is solved using an implicit Crank-Nicholson considering zero torques as boundary conditions, which is equivalent to consider zero densities as boundary conditions. We use 2000 radial bins logarithmically equally spaced that extend from the inner radius, $R_{\text{int}} = 0.1 (M_*/M_\odot)^{1/3}$ au, to 1000 au (Venturini et al. 2024).

For each value of the viscosity parameter α , the relation $\nu(\Sigma_g, R)$ for a star of a given mass (M_\star) and effective temperature (T_{eff}) is obtained from the resolution of the vertical structure of the disc taking into account the effects of the stellar irradiation (see Guilera et al. 2017, for a detailed description of the method). Due to the computational cost of solving the non-isothermal disc to perform a population synthesis with our model we implemented a grid of our vertical model in stellar mass and α parameter. We include stellar masses in the range 0.04 to $1.4 M_\odot$. We sample the continuum by taking intervals of $0.01 M_\odot$ in the range $0.04 - 0.1 M_\odot$, and $0.1 M_\odot$ in the range $0.1 - 1.4 M_\odot$. The parameter α takes discrete values in the range $10^{-5.5} - 10^{-1}$. We considered ten linearly spaced values in $\log \alpha$. To obtain the relation $\nu(\Sigma_g, R)$ for arbitrary values of α and M_\star , we use a bilinear interpolation in $\log \alpha$ and $\log M_\star$.

2.5.1. Internal photoevaporation by the central star

We consider X-ray (XR) and far ultraviolet (FUV) radiation from the central star, $\dot{\Sigma}_w = \dot{\Sigma}_{\text{XR}} + \dot{\Sigma}_{\text{FUV}}$.

The mass loss due to X-ray photoevaporation is computed following the analytical prescriptions by (Owen et al. 2012),

$$\dot{M}_{XR} = a \times 10^{-9} \left(\frac{M_*}{1M_\odot} \right)^b \times \left(\frac{L_{XR}}{10^{30} \text{erg s}^{-1}} \right)^{1.14} M_\odot \text{yr}^{-1}, \quad (7)$$

where $a = 6.25$ and $b = -0.068$ for the primordial disc stage. When a hole is fully opened in the inner part of the disc, $a = 4.8$ y $b = -0.148$. The XR luminosity is given by

$$\log(L_{XR} [\text{erg s}^{-1}]) = 30.37 + 1.44 \log \left(\frac{M_*}{M_\odot} \right). \quad (8)$$

The rate of FUV photoevaporation is computed following Kunitomo et al. (2021), where

$$\dot{\Sigma}_{FUV}(r \geq r_{FUV}) = \dot{\Sigma}_0 \left(\frac{L_{FUV}}{10^{31.7} \text{erg s}^{-1}} \right) \left(\frac{r}{4 \text{au}} \right)^{-2}, \quad (9)$$

and $\dot{\Sigma}_{FUV}(r < r_{FUV}) = 0$. $r_{FUV} = 4(M_*/M_\odot)$ au, and $\dot{\Sigma}_0 = 10^{-12} \text{g cm}^{-2} \text{s}^{-1}$. L_{FUV} is given by three main contributions, the luminosity produced by stellar accretion, that of the photosphere, and that of the chromosphere.

2.5.2. External photoevaporation

In star-formation regions massive stars dominate the production of UV radiation. Environments with high UV-radiation lead to photoevaporation from the outer region of the disc and play an important role in their evolution. Following Coleman & Haworth (2022), disc mass is considered to be removed from the gravitational radius $r_{g,fuv}$, and the mass loss rate by external photoevaporation is given by

$$\dot{\Sigma}_{\text{ext fuv}} = G_{sm} \frac{\dot{M}_d^{\text{fuv}}(r_d)}{\pi(r_{\text{max}}^2 - \beta^2 r_{g,fuv}^2)}, \quad (10)$$

where $\beta = 0.14$, r_{max} is the disc distance where $\Sigma_g(r) > 10^{-4} \text{g cm}^{-2}$, and \dot{M}_d^{fuv} is the mass loss rate for a disc of size r_d . The factor G_{sm} is a smoothing function around the effective gravitational radius,

$$G_{sm} = 1 - \left(1 + \left(\frac{r}{\beta r_{g,fuv}} \right)^{20} \right)^{-1}. \quad (11)$$

The mass-loss rate at 100 au is given by

$$\dot{M}_d^{\text{fuv}} = \dot{M}_0^{\text{fuv}} \frac{r_{\text{max}}}{100 \text{au}}, \quad (12)$$

where \dot{M}_0^{fuv} is a free parameter related to the intensity of the external UV radiation.

2.5.3. Disc viscosity

Within the α -disc framework (Shakura & Sunyaev 1973), the macroscopic kinematic viscosity ν is determined by the dimensionless parameter α . This parameter quantifies the degree of turbulence in the disc and is empirically calibrated to reproduce the observed accretion rates and disc lifetimes (e.g. Ribas et al. 2020). However, there is still no consensus on the most appropriate values of α when modeling protoplanetary discs. Values in the range 10^{-4} – 10^{-1} are typically required to reproduce the observed accretion rates (see Ribas et al. 2020, for a discussion).

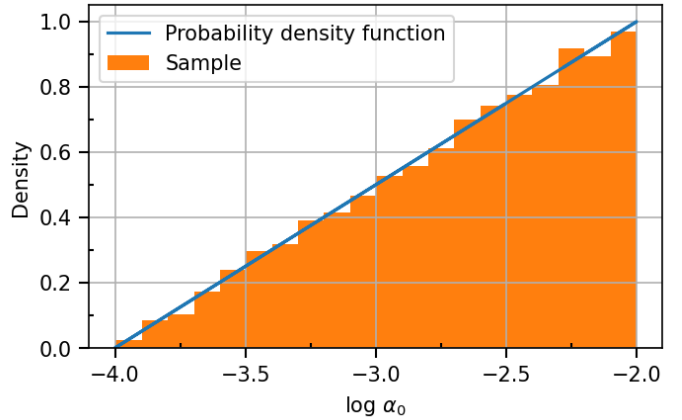


Fig. 3. Linear probability distribution for the $\log \alpha_0$ between -4 and -2. This distribution favors the presence of high viscosity discs in our population synthesis.

Observations also show that the stellar accretion rate is correlated with the stellar mass, approximately following $\dot{M} \propto M_\star^2$ (see Gorti et al. 2009, and references therein). It remains an open question whether this correlation is a consequence of disc evolution or merely reflects how the initial conditions scale with stellar mass (e.g. Ercolano & Pascucci 2017; Manara et al. 2023). Following Gorti et al. (2009), we assume that the correlation arises from the dependence of the turbulent properties of the disc on stellar mass, such that $\alpha = \alpha(M_\star)$.

To account for the observed dispersion in the accretion rates at a given stellar mass, we follow Manara et al. (2023) and introduce a dispersion in α by means of an auxiliary parameter α_0 , such that

$$\alpha = \alpha_0 \times M_\star^a,$$

where a is a free parameter to be calibrated. We explore the effect of adopting two different distributions for α_0 : a uniform distribution and a linear one. In the latter case, for a given stellar mass, more viscous discs are more likely to occur around higher-mass stars.

Regarding the range of α_0 , we consider two cases: $\log \alpha_0 \in [-4.0, -2.0]$ and $\log \alpha_0 \in [-3.5, -1.5]$. Fig. 3 illustrates an example of the linear probability density function for $\log \alpha_0$. In this scenario, high-viscosity discs are favored—rather than being uniformly distributed—for a given stellar mass.

3. Observational constrain disc evolution models

The observations of protoplanetary discs provide important constraints on their properties and evolution. The fraction of stars with discs as a function of the young stellar cluster ages, the masses of the discs, their dissipation timescales, and the accretion rates onto the central stars are some of the most important observational constraints currently available.

For this work, we consider the statistical sample obtained by Manara et al. (2023) of the stellar mass accretion rates as a function of the disc masses and as a function of the stellar masses for almost 1000 young stellar objects within 300 pc. The sample contains young stellar clusters at different evolutionary stages and environments. The stellar mass accretion rates as a function of the disc masses are inferred from the dust disc masses from Manara et al. (2019) using the standard dust-to-gas ratio of 1% similar to the interstellar medium (in App. B we analyze the impact of different values for the dust-to-gas ratio).

In addition, to constrain the lifetime of the protoplanetary discs, we considered the result from Pfalzner et al. (2022). The observations of clusters closer than 200 pc, wherein all the stellar mass distribution can be well estimated, allow one to obtain median disc lifetime between 5 – 10 Myr. Clusters at larger distances seem to underestimate the contribution of low-mass stars, deriving short disc lifetimes of about 1 – 3 Myr. The main reason for this discrepancy is that distant clusters are affected by a limiting magnitude, thus in the samples of distant clusters low-mass stars are underrepresented. In order to compare the observed fraction of stars with discs depending on the cluster distances (Pfalzner et al. 2022), we implement in our population synthesis a cut-off in our mass distribution, mimicking a limiting magnitude due to the cluster distances.

4. Results

We present the results of our simulations by comparing synthetic disc population models with available observational data. Our analysis focuses on disc lifetimes as a function of host star properties and local formation conditions. Observations of disc fractions in stellar clusters of varying ages suggest that typical protoplanetary discs have lifetimes ranging from 1 to 10 Myr. In addition, for each synthesis, we extract key observables: disc lifetimes inferred from the disc-star fraction over the 1–20 Myr age range, and mass accretion rates onto the central star as functions of both disc mass and stellar mass at 1.5 Myr –a representative age for young clusters such as Taurus, Lupus, and Chamaeleon I–. In order to compare the simulations against the observations, we compute the mass accretion onto the star as

$$\dot{M}_{acc} = 2\pi R \Sigma_{gas}(R) v_{gas}(R), \quad (13)$$

$v_{gas}(R)$ being the gas radial velocity (see Gárate et al. 2020). We note that for comparison, \dot{M}_{acc} is computed in the innermost part of the disc.

To assess the impact of the limiting detection magnitude on the inferred mean disc dissipation times –derived from the fraction of stars with discs as a function of cluster age–, we performed a series of simulations using different lower limits for the stellar mass distribution. To analyze the effect of adopting a simplified star formation rate (SFR), we considered two scenarios: one in which all stars form simultaneously within the cluster, and the other in which star formation follows a temporal distribution characterized by a timescale of $t_d = 1$ Myr.

4.1. Reference synthesis

We first generate a population of 10000 star–disc systems, with model parameters drawn from distributions inferred from observations, as described in the previous section. In this reference synthesis, we assume the α -viscosity parameter follows a uniform distribution in logarithmic space between $\log \alpha = -4$ and $\log \alpha = -2$, consistent with typical values used to reproduce observed disc properties (e.g. Ribas et al. 2020; Rosotti 2023).

The main results of the reference synthesis are shown in Fig. 4. The top row displays the results assuming all star–disc systems begin their evolution simultaneously at time zero (i.e., without considering a prolonged SFR), while the bottom row presents the same results incorporating a time-dependent SFR.

The left column of Fig.4 shows the fraction of stars with discs as a function of cluster age. The data points represent observed disc fractions with their associated uncertainties. Blue

points correspond to clusters within 200pc, green to those between 200–500pc, and orange to clusters between 500–1000pc (Pfalzner et al. 2022). The red line shows the disc fraction fit for a low-mass star-corrected sample from Pfalzner et al. (2022), while the black line shows the classical fit from Mamajek (2009). The latter may overestimate the contribution of massive stars, as it does not account for cluster distance effects (see Pfalzner et al. 2022; Pfalzner & Dincer 2024).

Our synthetic results are shown as dashed lines. To mimic the varying stellar mass completeness across clusters at different distances, we apply different lower limits on the stellar mass when computing disc fractions. The blue dashed line represents the full synthetic population, spanning stellar masses from $0.04 M_{\odot}$ to $1.4 M_{\odot}$. This model underestimates the disc fractions in clusters where low-mass stars are well sampled (cf. red line). Notably, we observe a steep decline in disc fractions at early ages, with a mean synthetic disc lifetime of ~ 3 Myr.

When applying higher mass cut-offs to reflect observational biases at greater distances –specifically, 0.1 and $1.0 M_{\odot}$ for the green and orange dashed lines, respectively–, we observe an even lower disc fraction, consistent with the faster disc dispersal around massive stars (e.g. Ribas et al. 2015). A mass threshold of $1 M_{\odot}$ is required to reproduce the disc fractions reported by Mamajek (2009) and those observed in distant clusters (500 to 1000 pc) (Pfalzner et al. 2022).

When the SFR is included in the calculation of the fraction of stars with discs (bottom-left panel of Fig. 4), we observe an increase in the number of disc-bearing stars at young cluster ages. The inclusion of the SFR shifts the median disc lifetimes to ~ 4.0 Myr, consistent with the results reported by Coleman & Haworth (2022). This increase is attributed to ongoing star formation during the first few million years, which populates the clusters with newly formed stars still hosting protoplanetary discs.

The central panels of Fig.4 show a color density map (i.e. the number of systems per pixel) of the stellar mass accretion rate as a function of the gas disc mass when the age of the cluster is 1.5 Myr. The orange, magenta, pink and red points correspond to the observed disc masses in the star-forming regions of Chameleon I, Lupus, Taurus and Ophiuchus, respectively, and considering a classical dust-to-gas ratio of 1% Manara et al. (2023). The dashed-dot lines represent different dispersal timescales, $\tau = M_{gas}/\dot{M}$, of 0.1 , 1 and 10 Myr. Without considering a SFR (top-central panel), high accretion rates for intermediate- and large-mass discs, and all the range of accretion rates for low-mass discs are not able to reproduce. In order to better reproduce the observations for low-mass discs and high accretion rates is necessary to introduce a prolonged SFR. The inclusion of a SFR affects the accretion rate–disc mass relation by shifting systems above the dissipation timescale curves $\tau = M_{gas}/\dot{M}$. This shift is primarily driven by the continuous formation of young star–disc systems during the first few million years, which introduces low-mass discs with relatively high accretion rates. As a result, the inclusion of the SFR increases the scatter in both the $\dot{M}-M_{gas}$ and $\dot{M}-M_{\star}$ correlations. This additional dispersion tends to improve the agreement between the synthetic accretion rates and those observed in young stellar populations. However, we are not still able to match the observed accretion rates for low-mass discs.

The right column of Fig. 4 displays the stellar mass accretion rate as a function of the stellar mass. Observational data from young stellar clusters are shown again as orange, magenta, pink, and red points. The orange line represents the observational fit, $\dot{M}_{obs} \propto M_{\star}^{1.8}$, as reported by Manara et al. (2023). The corre-

sponding trend from our synthetic population is shown as a gray curve. Due to the overproduction of low-mass stars with high accretion rates in our models, the resulting correlation between \dot{M} and M_\star appears flatter than the observed one. Consequently, neither of our population synthesis models—whether incorporating an SFR or not—successfully reproduces the observed $\dot{M}-M_\star$ relation.

4.2. Disc viscosity as a function of the stellar mass

The results presented in the previous section highlights the necessity to incorporate a correlation between the disc viscosity and the stellar mass. In addition, such correlation can be inferred from the observations of the stellar mass accretion rate as a function of the stellar mass, which lead to a relation $\dot{M}_{\text{obs}} \propto M_\star^{1.8}$ (Manara et al. 2023). Thus, under the assumption that the disc viscosity is correlated with the stellar mass, we calculate new population synthesis considering a correlation for the α -viscosity parameter of the form $\alpha = \alpha_0 \times M_\star^a$. We also consider two different distributions for α_0 : first we adopt that $\log \alpha_0$ follows a uniform distribution; then we assume a linear distribution (see previous section). For our population synthesis we consider three values for the stellar mass exponent $a = 1.5, 1.8$, and 2.0 .

4.2.1. $\log \alpha_0$ between -4 and -2

In Fig. 5 we show the results of our synthesis considering $\log \alpha_0$ in the range -4 to -2 and the value of $a = 1.8$ (the results for the synthesis adopting $a = 1.5$ and 2 are detailed in App. A.1). The top panels show the results of considering the uniform probability distribution for $\log \alpha_0$, while the bottom panels the result of considering the proportional probability distribution for $\log \alpha_0$. In both cases we consider a SFR. As in Fig. 4, the first column shows the fraction of stars with discs as a function of the time.

Including a viscosity dependence on stellar mass results in synthetic disc fractions that very well match the estimations of Pfalzner et al. (2022) in both cases, specially for cluster ages larger than ~ 5 Myr. In addition, we find that mean synthetic disc lifetime is independent of the α_0 distribution, being ~ 5 Myr. When we apply a mass cut-off at $1 M_\odot$, to mimic in someway the observational biases at larger cluster distances, our synthetic disc fractions also reproduce the disc lifetimes inferred by Mamajek (2009), and the observed disc fractions of young stellar clusters with distances larger than 500 au.

The accretion rate as a function of the disc mass is shown in the central column. Due to the correlation between the α -viscosity parameter with the stellar mass, we can see that low- and moderate-mass discs show a decrease in the mass accretion rates, not being able to reproduce the observations.

As in Fig. 4, the accretion rate as a function of the stellar mass is shown in the right column. Adopting a stellar mass dependence for the disc viscosity, both distributions show an agreement on the correlation between the synthetic $\dot{M}-M_\star$ results and the observations. Considering a linear distribution for $\log \alpha_0$ leads to a better agreement against the observations of our disc population synthesis. However, it is evident that the synthetic accretion rates are considerably lower than those estimated by the observations, with a considerable degree of dispersion in the values.

4.2.2. $\log \alpha_0$ in the range -3.5 to -1.5

In the previous section we showed that if the disc viscosity is proportional to the star mass, the trend in the observed correlation $\dot{M}-M_\star$ can be recovered. However, the synthetic accretion rates are smaller than the observed ones. With the aim to obtain larger synthetic accretion rates from our population, we examine a new synthesis adopting a higher range for the $\log \alpha_0$. In particular, we adopt a range between -3.5 and -1.5 for $\log \alpha_0$. As in the previous section, we consider two population synthesis, one following a uniform distribution, and the other assuming a linear distribution between -3.5 and -1.5. The results considering $a = 1.8$ are shown in Fig. 6. The results for the synthesis adopting $a = 1.5$ and 2 are detailed in App. A.2. Despite the increment in the range of the values for the α_0 -viscosity parameter, we note that since the distribution of α is weighted by the stellar mass the effective range of α is between $\sim 5 \times 10^{-5}$ and $\sim 6 \times 10^{-2}$.

The left panels of Fig. 6 show that our results satisfactorily reproduce the fraction of stars with discs for clusters with distances less than 200 pc considering both $\log \alpha_0$ distributions. The mean synthetic disc lifetime of both population synthesis are ~ 4 Myr. Also in both cases, considering a limiting stellar mass of $1 M_\odot$ for the population allows us to reproduce the results obtained by Mamajek (2009).

In the right panels Fig. 6, we plot again the stellar mass accretion rate as a function of the star mass. We find that the increment in the values of $\log \alpha_0$ generates that both distributions reproduce very well the observational trend of $\dot{M}-M_\star$. In particular, when we consider a linear distribution for the $\log \alpha_0$ we get a very good agreement with the observations, reproducing very well the observed correlation $\dot{M}_{\text{obs}} \propto M_\star^{1.8}$, and the magnitudes and dispersion of the observed stellar mass accretion rates.

However, as seen in the central panels of Fig. 6, we still fail to reproduce the stellar mass accretion as a function of the gas disc mass. None of the synthetic populations are able to efficiently generate low- and intermediate-mass discs with high accretion rates. We note however, that one possibility to better reproduce this observational estimations is to consider a large solid-gas ratio which leads to large gas disc masses. At 1.5 Myr, a significant amount of solids of the disc could be in larger objects, whose sizes do not contribute to the infrared observations. Other possibility is to consider a phenomenon—as external photoevaporation—that could reduce gas disc masses maintaining high accretion rates.

4.3. The impact of environmental conditions

The correlations between stellar mass accretion rates and disc masses arises naturally within the framework of viscous disc evolution. Initially, the model deals with intermediate- massive-discs with high accretion rates. As discs evolve, disc masses and mass accretion rates decrease. The accretion rates vanish for low-mass discs because of the internal photoevaporation. Internal photoevaporation opens an inner hole when it is effective, cutting-off the accretion for low-mass discs. This picture is clearly not in full agreement with the observations of young stellar clusters which show low-mass discs with high accretion rates.

On contrary, when external photoevaporation is considered in the model, the discs lose material from the external region, where the external radiation is effective (Coleman & Haworth 2022), while the internal part of the disc evolves mainly by accretion and internal photoevaporation, allowing to reach high accretion rates even for low-mass discs.

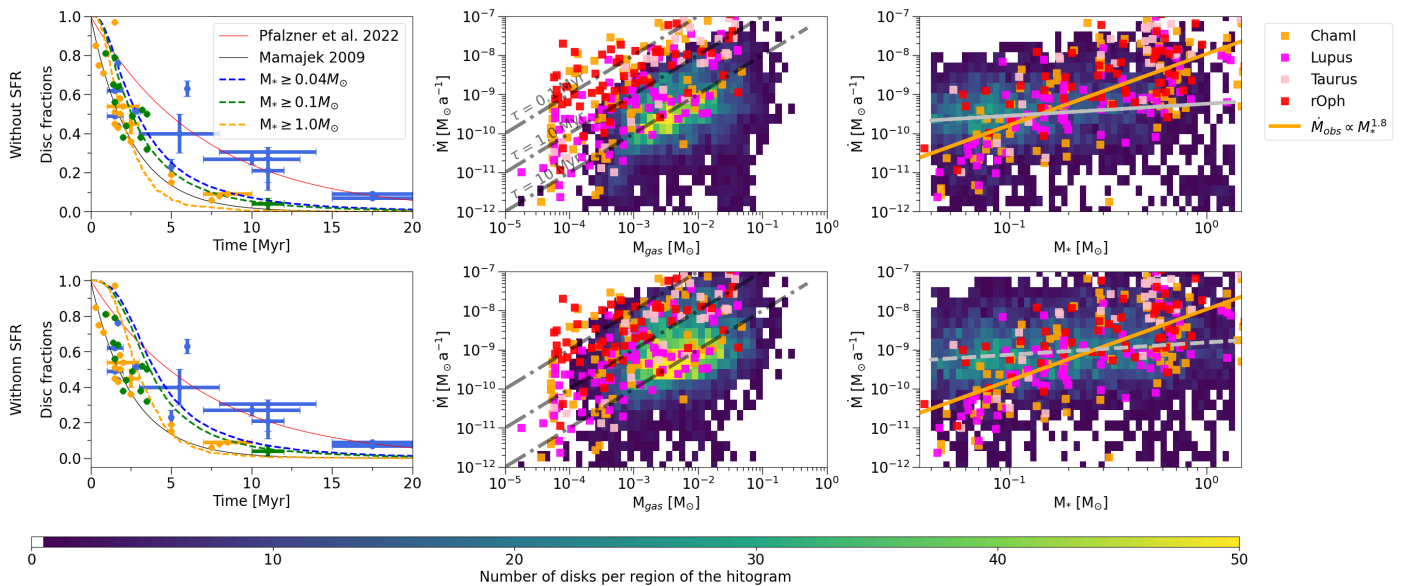


Fig. 4. Top panels. Disc population synthesis results without considering a prolonged SFR. Bottom panels. Results adopting a SFR with a characteristic timescale $t_d = 1$ Myr. Left column. Fraction of stars with discs as a function of the age of the cluster. Blue, green and orange points correspond to observations of young stellar clusters within 200 pc, between 200–500 pc and between 500–1000 pc, respectively. The red line represents the fit to cluster within 200 pc (Pfalzner et al. 2022). The black line corresponds to the results obtained by Mamajek (2009). The dashed lines represent the results of our population synthesis for different values of the minimum stellar mass considered. The orange, green and blue dashed lines correspond to the minimum stellar masses of $M_{*,m} = 1, 0.1$ and $0.004M_\odot$, respectively. Center column. Histogram (or color density map) for the stellar mass accretion rate as a function of the disc mass at 1.5 Myr from the population synthesis. Orange, magenta, pink, and red points represents the observations compiled in Manara et al. (2023). Right column. Stellar mass accretion rate against stellar mass, also at 1.5 Myr of the synthesis evolution. The orange line represents the fit to the observations (Manara et al. 2023), while the gray line is the fit to our results.

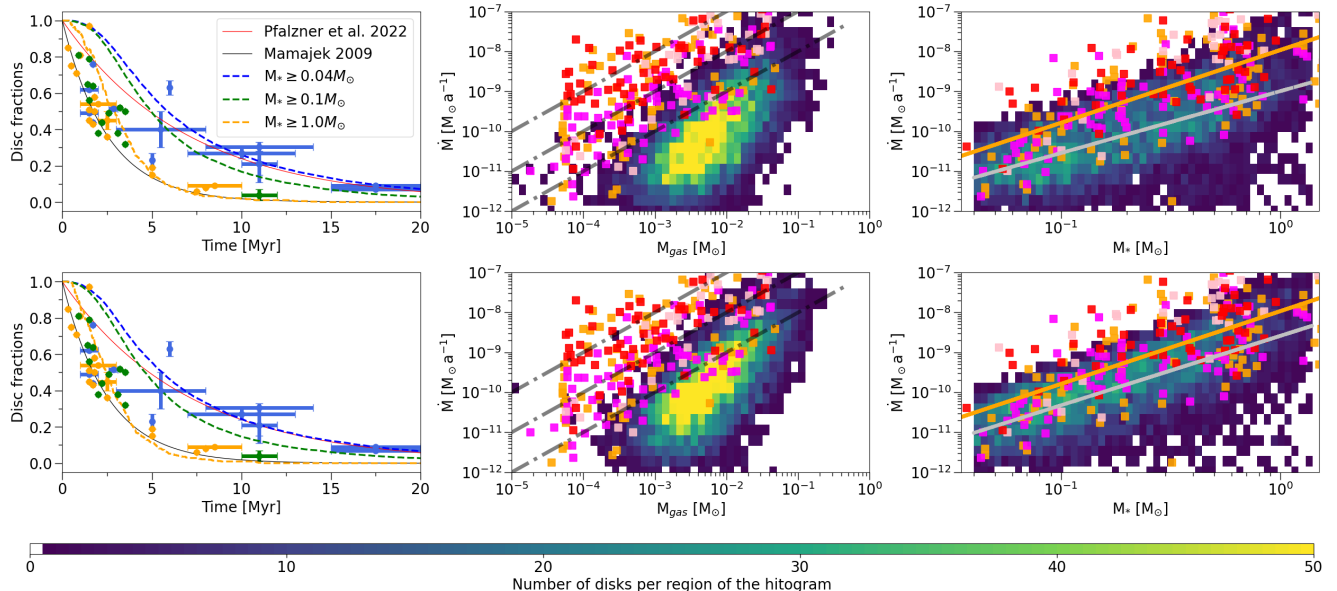


Fig. 5. Similar to Fig. 4, but considering the α -viscosity parameter as a function of the stellar mass ($\alpha = \alpha_0 \times M_*^{1.8}$) and considering a SFR with $t_d = 1$ Myr. The top row corresponds to the results for the population synthesis adopting a uniform distribution for α_0 , while the bottom row corresponds to consider a linear distribution for α_0 . In both cases the range of the $\log \alpha_0$ is between -4 and -2.

Thus, we compute a new disc population synthesis including external photoevaporation with the aim to also reproduce the observed trend for the accretion rate as a function of the disc mass. We consider that $\log \alpha_0$ follows a linear distribution in the range between -3.5 and -1.5. For the external photoevaporation mass loss rate, we consider a moderate UV radiation environment with a mass-loss rate of $\dot{M}_0^{\text{fuv}} = 2 \times 10^{-8} M_\odot \text{ y}^{-1}$, corresponding to about $2000 G_0$ (Coleman & Haworth 2022).

The main results of the synthesis adopting $\alpha = 1.8$ (in the relation $\alpha = \alpha_0 \times M_*^a$) are shown in Fig. 7. As in previous figures, the left panel shows the fraction of stars with discs. The points and their corresponding error-bars highlight the observation estimations for the young stellar cluster (Ribas et al. 2015; Pfalzner et al. 2022) from which we have also estimations of the accretion rates (Manara et al. 2023). The dashed blue line corresponds to the full star population of our synthesis, i.e. considering the stars

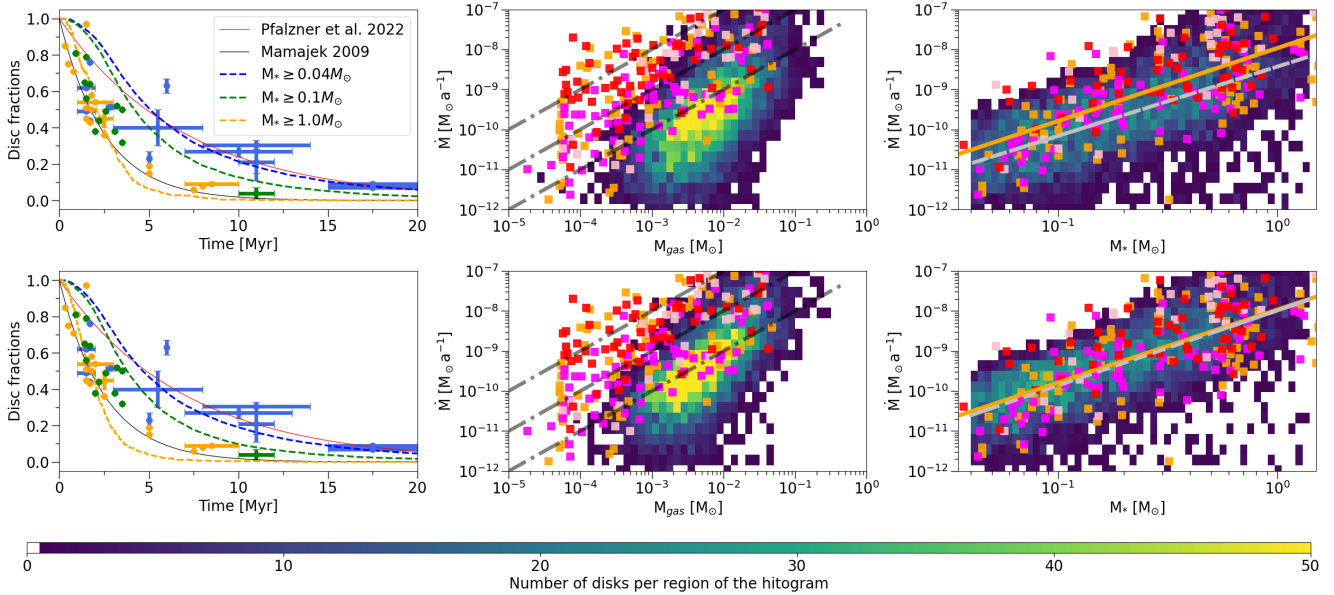


Fig. 6. Same as Fig. 5, but considering the range of the $\log \alpha_0$ between -3.5 and -1.5.

between $0.04 M_\odot$ and $1.4 M_\odot$, taking into account the external photoevaporation. The grey dashed line corresponds to the same synthesis without the external photoevaporation. We can see that the inclusion of this phenomenon helps to better reproduce the fraction of stars with discs in the young stellar cluster, considering the full star sample of the synthesis.

In addition, we can see in the central panel of Fig. 7 that the inclusion of the external photoevaporation is a fundamental piece to reproduce the observed stellar mass accretion rates as a function of the disc masses. As we mention before, the external photoevaporation is a key phenomenon to reduce the mass of the disc from the outer regions, leaving high surface densities in the inner part of the discs, generating low-mass discs with high accretion rates.

Finally, we remarkably note that the synthetic accretion rates as a function of the stellar masses are practically not affected by the external photoevaporation (right panel of Fig. 7). Our synthesis reproduce again very well the observed correlation $M_{\text{obs}} \propto M_\star^{1.8}$ (including the magnitudes and dispersion of the observed accretion rates).

Thus, to reproduce the observed accretion rates in young clusters, for which the disc mass is inferred, it is necessary to consider the effect of the environment produced by the external photoevaporation. Contrary, in order to reproduce the extended-lived discs also observed in near clusters, no external radiation is required. In addition, in the case of discs with high accretion rates at extended ages, as is the case of Upper Scorpius, it is necessary to consider an extended star formation rate, which is supported by the observations (see next section).

4.3.1. The interesting case of Upper Scorpius

In this section, we look for the initial conditions of our model that allow us to reproduce the observable characteristics of the young stellar cluster Upper Scorpius. This cumulus appears to be older than the previously studied, with an estimated age between ~ 5 Myr and ~ 11 Myr (Fang et al. 2017; Squicciarini et al. 2021; Manara et al. 2023). Upper Scorpius presents a non-negligible number of components with high accretion rates despite its estimated age, with a high $\dot{M} - M_{\text{disc}}$ dispersion.

In order to reproduce observations, we need to consider a large characteristic time of the star formation rate of 5 Myr, and as in Sec. 4.3 we consider that the simulations are affected by a moderate FUV external photoevaporation (in order to be able to reproduce low-mass discs with high accretion rates). The Fig. 8 represents the results of our synthesis. Central and right panels, represent the stellar mass accretion rates as a function of the disc masses and as a function of the star masses, respectively, at 11 Myr of the synthesis evolution. Our results show that substantial accretion rates can still be present in an evolved cluster such as Upper Scorpius, if a prolonged star formation history is taken into account. Conversely, if a star formation history is not considered in the modeling, our simulations show that by 11 Myr, all discs have dissipated and no accreting stars remain in the population. In addition, if FUV external photoevaporation is not also considered, we can not account for low-mass discs with high accretion rates.

The left panel of Fig. 8 shows the fraction of stars with discs as a function of the time. We can see that our synthesis match also well the observed disc fraction estimations (Ribas et al. 2015; Pfalzner et al. 2022). As we mentioned before, the age of Upper Scorpius remains uncertain. Squicciarini et al. (2021) suggest that the discrepancy in the age estimation could be partially explained by an intrinsic age spread within the region. Such age spreading could account for the relatively high number of accreting stars observed, in agreement with our results. In addition, our synthetic fraction of stars with disc is closer to the estimations for the clustered and diffuse components given by Squicciarini et al. (2021).

5. Summary and Discussion

In this work we performed disc population synthesis adopting initial conditions inferred from the observations and considering that discs evolve by viscous accretion, X-ray internal photoevaporation, and in some cases UV external photoevaporation.

In previous sections, we analysed and explored how disc initial conditions affect some important disc observations. In particular, we aimed to reproduce the fraction of stars with discs,

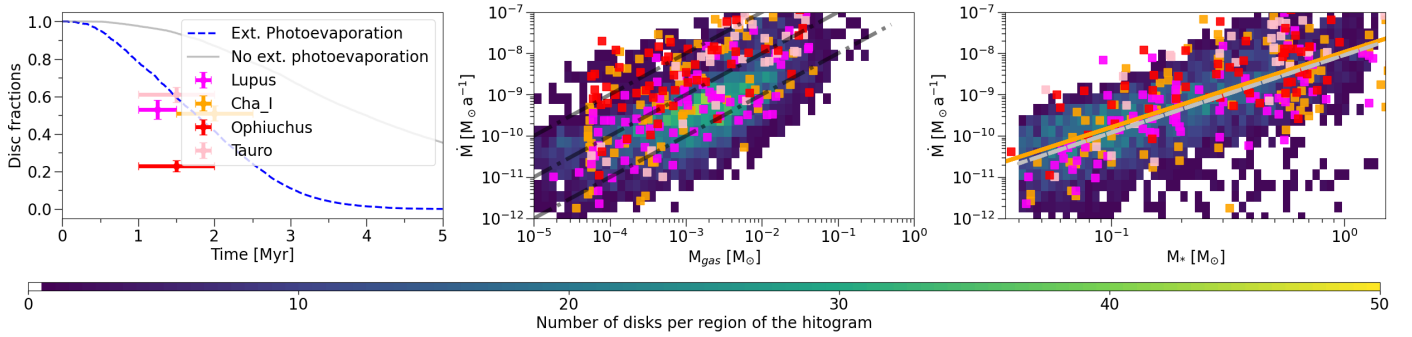


Fig. 7. Population synthesis results considering a linear distribution of the $\log \alpha_0$ between -3.5 and -1.5, $a = 1.8$ and considering that population is affected by external photoevaporation. The grey line in left panel represents the fraction of stars with discs for the population synthesis where external photoevaporation is not considered.

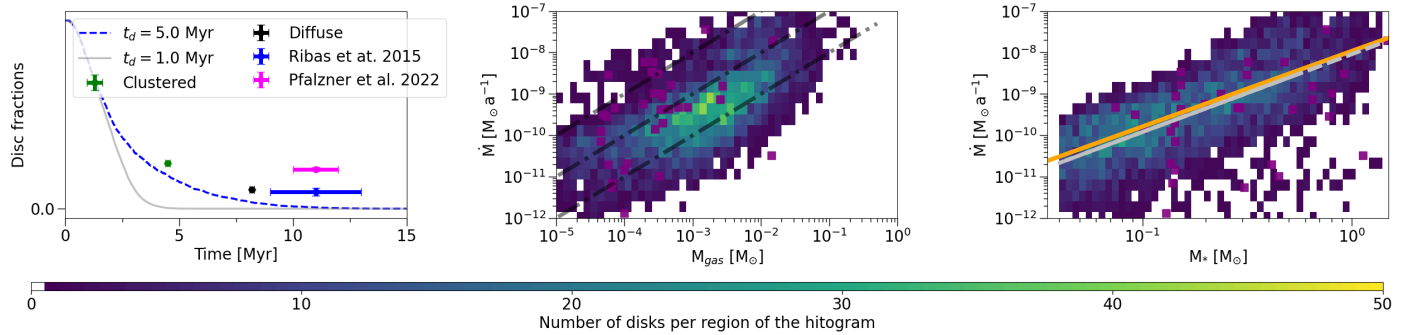


Fig. 8. Same as Fig. 7 but adopting an extended star formation rate with $t_d = 5$ Myr. As comparison, the grey line in the left panel corresponds to the synthesis results adopting $t_d = 1$ Myr. The purple dots correspond to the observational data from Manara et al. (2023) for the Upper Scorpius cluster. The color dots represent our synthetic accretion rates at 11 Myr of the synthesis evolution.

and the stellar mass accretion rates as a function of the stellar masses and disc masses inferred for young stellar clusters.

We first showed that in order to better reproduce the observed fraction of stars with discs in near young stellar clusters within 200 pc (estimated by Pfalzner et al. 2022), a star formation rate plays a fundamental role (left panels of Fig. 4). We also showed that if we apply a cut-off in the stellar mass distribution (mimicking in somewhat the incompleteness of the full star population due to cluster distances), we were able to match the estimations from Mamajek (2009) and the disk fractions for stellar clusters located farther than 500 pc (Pfalzner et al. 2022).

A key result of this work is that in order to reproduce the observational trend between the stellar mass accretion rates and the stellar masses in young clusters (e.g. Muzerolle et al. 2000; Natta et al. 2006; Manara et al. 2023), we needed to impose a correlation between the disc viscosity and the stellar mass. Following previous theoretical works that already implemented such correlation based on an observational necessity (e.g. Gorti et al. 2009), we adopted that the α -viscosity parameter scale with the stellar mass as $\alpha = \alpha_0 (M_*/M_\odot)^a$. We found that adopting $a = 1.8$ following the observational correlation, and if $\log \alpha_0$ follows a linear distribution in the range between -3.5 to -1.5, the synthetic accretion rates as a function of the stellar masses are in very good agreement with the observations (right-bottom panel of Fig. 6). Such values of α_0 correspond to values of α between $\sim 5 \times 10^{-5}$ (for the less massive stars) and $\sim 6 \times 10^{-2}$ (for the more massive stars).

Finally, we also found that in order to reproduce the observed accretion rates as a function of the gas discs masses, the inclusion of UV external photoevaporation radiation becomes fundamental. Assuming a moderate radiation environment our synthe-

sis are effective in generate low-mass discs with high accretion rates, and the synthetic accretion rates as a function of the gas disc masses reproduce very well the observations (central panel of Fig. 7). In addition, the synthetic fraction of stars with discs remarkably matches the observed ones for the clusters of Lupus, Chameleon I, and Taurus, as well as the accretion rates as function of the stellar masses inferred for these young stellar clusters (left and right panels of the Fig. 7, respectively).

5.1. Comparison with previous studies

Our results reinforce and expand upon several previous findings regarding protoplanetary disc evolution. One key point is the observed large scatter in the correlation between mass accretion rate and stellar mass. This dispersion has been long noted in the previous works (e.g. Manara et al. 2023), and our model successfully reproduces it by introducing a distribution in the α -viscosity parameter α_0 , as well as a dispersion in the initial disc mass distribution. The synthetic mass accretion rate of our model, given by Eq. (13), links the mass accretion rate to both the surface density and the gas radial velocity, which are in turn controlled by α -viscosity parameter. Without a dependence of α on stellar mass, our simulations predict a nearly flat $\dot{M} - M_*$ relation (as in Fig. 4), which underestimates the observed correlation. However, by introducing a scaling of the form $\alpha \propto M_*^a$, with $a = 1.8$, we are able to recover the observed trend (Gorti et al. 2009; Manara et al. 2023).

Additionally, our population synthesis results confirm the importance of observational biases due to limiting magnitudes, as highlighted by Pfalzner et al. (2022). These biases lead to an over representation of massive stars in distant clusters, arti-

ficially shortening the inferred average disc lifetimes. By mimicking such biases through a stellar mass cut-off in our models, we reproduce both the longer disc lifetimes in nearby clusters ($\gtrsim 5$ Myr) and the shorter ones inferred in more distant systems (~ 1 – 3 Myr). Furthermore, our findings align with those of Ribas et al. (2014) and Emsenhuber et al. (2023), who showed that low-mass stars retain their discs longer when evolving in isolation due to reduced internal photoevaporation. This long-lived disc population may be associated with the so-called *Peter Pan* discs (Coleman & Haworth 2022), which our model naturally reproduces under conditions of low α and weak external FUV stellar photoevaporation.

A particularly relevant point of comparison is with the study of Emsenhuber et al. (2023), who used a similar model to study the disc properties in nearby star-forming regions. Their models indicated that the combined effect of internal and external photoevaporation tends to disperse discs too quickly to match the observed fraction of stars with discs, especially in the cluster of Lupus and Chamaeleon I. To address this, they adopted initial conditions with more massive, compact discs and omitted external photoevaporation entirely.

In contrast, our results show that moderate external photoevaporation –when appropriately modeled– is not only compatible with the observed disc lifetimes but also essential to reproduce low-mass discs with high accretion rates. In our synthesis, external photoevaporation acts preferentially on the outer disc, leaving high surface densities in the inner regions and thus allowing high accretion rates even in low-mass discs –a trend commonly observed in young clusters.

Moreover, Emsenhuber et al. (2023) adopt a constant α across the stellar mass distribution. This choice fails to reproduce the observed $\dot{M} - M_*$ correlation. In contrast, we introduce a dependence of α on M_* , allowing our synthetic populations to recover both the slope and scatter of the observed correlation. We also find that a linearly biased distribution of $\log \alpha_0$ toward higher viscosities further improves agreement with observations.

Another important distinction is our explicit implementation of a time-dependent star formation rate. By incorporating an exponentially declining SFR with a timescale of $t_d = 1$ Myr, we recover the observed increase in disc fractions at early cluster ages. This contrasts with the absence of a SFR assumption in Emsenhuber et al. (2023), which limits the model’s ability to reproduce age-dependent trends in disc demographics.

Altogether, while both approaches capture aspects of the observed disc population, our study demonstrates that including a stellar-mass-dependent viscosity, extended star formation histories, and moderate external photoevaporation is necessary to simultaneously match the observed distributions of \dot{M} , M_{gas} , and disc lifetimes across various environments.

5.2. Implications for planet formation

The diversity of exoplanetary systems observed to date likely reflects the interplay between stellar mass, disc evolution, and environmental effects. Our simulations suggest that different disc dissipation timescales, viscosity regimes, and accretion histories naturally lead to distinct planetary system architectures.

In high-viscosity discs, in our model associated with more massive stars, the combination of rapid viscous evolution and intense internal (and also external) photoevaporation compresses the timescales available for planet formation. On the contrary, these discs are also the more massive ones, favoring for example the formation of gas giants. In fact, occurrence rates of giant planets grow with the stellar mass (see for example Pan et al.

2025). Thus, if giant planets form via core accretion, this implies that massive solid cores should form quickly enough. However, high levels of turbulence can also enhance the collisional fragmentation of small solids and increase their radial diffusion, potentially inhibiting the efficient growth of pebbles and planetesimals. In addition, in the context of pebble accretion, high-viscosity environments reduce the efficiency of pebble accretion (e.g. Venturini et al. 2020a). This effect can act as a bottleneck for the rapid formation of massive cores before the gas disc dissipates, making giant planet formation more difficult unless pebble fluxes are exceptionally high.

Conversely, low-viscosity discs –often found around low-mass stars in our model– evolve more slowly and are less affected by both internal and external photoevaporation. These discs offer extended lifetimes, which are favorable for the gradual formation of rocky planets, super-Earths, and also possible sub-Neptunes. The reduced turbulence in such environments promotes pebble settling toward the mid-plane, increasing their local density and enhancing pebble accretion efficiency (e.g. Venturini et al. 2020a). Furthermore, our results support the idea that external photoevaporation can selectively truncate the outer disc while preserving the high surface density of the inner regions. This configuration can maintain high accretion rates in low-mass discs and may favor the formation of compact, tightly packed planetary systems, similar to those observed in systems like TRAPPIST-1 or Kepler-42.

Taken together, our findings reinforce the notion that the architecture and diversity of planetary systems are deeply influenced by the interplay between stellar mass, disc viscosity, and environmental conditions. Disc population synthesis models that include these dependencies are thus key to bridging the gap between disc observations and the diversity of known exoplanets.

6. Conclusions

One of our main results is that, if discs evolve through viscous accretion and photoevaporation, internal and/or external, it is essential to include a correlation between the disc viscosity and the stellar mass to reproduce the observed correlation between the stellar mass accretion rates and the stellar masses. It remains to be seen whether a physical mechanism with these characteristics can be found. In addition, our synthetic correlation between the stellar mass accretion rates and the stellar masses remains invariant in time, in line with the observational estimations.

Furthermore, to explain the observed high accretion rates, it is necessary to consider a probability distribution that favors discs with high viscosity. It is also crucial to incorporate a star formation rate over approximately one million years in order to reproduce the high accretion rates associated with massive stars in clusters around 1–2 Myr. The high accretion rates observed in cumulus clusters with extended ages, such as Upper Scorpius, are explained by an extended star formation. Our disc population synthesis is able to reproduce the observations on Upper Scorpius adopting a formation rate of ~ 5 Myr. Additionally, including a star formation rate explains the observed dispersions in accretion rates and also leads to the observation of high accretion rates in moderate and high mass discs. However, in both cases –for very young stellar clusters of ~ 1 – 2 Myr or for older clusters like Upper Scorpius– to be able to reproduce the high accretion rates observed in low-mass discs, it is fundamental to consider external photoevaporation.

Finally, we find that our synthetic population in which disc viscosities are correlated with stellar masses, are able to reproduce the estimated ages of protoplanetary discs –ranging from

1 to 20 Myr–, and the fraction of stars with discs observed in young stellar clusters. In addition, cutting off the minimum stellar mass of our population (mimicking the distances to the different young stellar clusters and the observational stars mass limit) we are also able to reproduce the different observational estimations of the disc fractions for young stellar clusters at different distances.

Acknowledgements. We thanks Alexander Emsenhuber, Remo Burn and Jesse Weder for usefull discussion during the development of this work. This work is partially supported by PIP 2971 from CONICET (Argentina) and by PICT 2020-03316 from ANPCyT (Argentina). We also thank Juan Ignacio Rodriguez from IALP for the computation managing resources of the Grupo de Astrofísica Planetaria de La Plata.

Rosotti, G. P., Tazzari, M., Booth, R. A., et al. 2019, *Monthly Notices of the Royal Astronomical Society*, 486, 4829
 Sellek, A. D., Booth, R. A., & Clarke, C. J. 2019, *Monthly Notices of the Royal Astronomical Society*, 492, 1279
 Shakura, N. I. & Sunyaev, R. A. 1973, *Astronomy and Astrophysics*, 24, 337
 Squicciarini, V., Gratton, R., Bonavita, M., & Mesa, D. 2021, *MNRAS*, 507, 1381
 Suzuki, T. K. & Inutsuka, S.-i. 2009, *ApJ*, 691, L49
 Tazzari, M., Testi, L., Natta, A., et al. 2017, *A&A*, 606, A88
 Tychoniec, Ł., Tobin, J. J., Karska, A., et al. 2018, *The Astrophysical Journal Supplement Series*, 238, 19
 Venturini, J., Guilera, O. M., Ronco, M. P., & Mordasini, C. 2020a, *A&A*, 644, A174
 Venturini, J., Ronco, M. P., & Guilera, O. M. 2020b, *Space Sci. Rev.*, 216, 86
 Venturini, J., Ronco, M. P., Guilera, O. M., et al. 2024, *A&A*, 686, L9

References

Andrews, S. M., Wilner, D. J., Hughes, A. M., Qi, C., & Dullemond, C. P. 2010, *The Astrophysical Journal*, 723, 1241
 Armitage, P. J. 2009, *Protoplanetary disk evolution* (Cambridge University Press), 65–108
 Blandford, R. D. & Payne, D. G. 1982, *MNRAS*, 199, 883
 Coleman, G. A. & Haworth, T. J. 2022, *Monthly Notices of the Royal Astronomical Society*
 Drązkowska, J., Bitsch, B., Lambrechts, M., et al. 2022, arXiv preprint arXiv:2203.09759
 Emsenhuber, A., Burn, R., Weder, J., et al. 2023, arXiv preprint arXiv:2301.04656
 Emsenhuber, A., Mordasini, C., Burn, R., et al. 2021, *A&A*, 656, A70
 Ercolano, B. & Pascucci, I. 2017, *Royal Society Open Science*, 4, 170114
 Fang, Q., Herczeg, G. J., & Rizzuto, A. 2017, *ApJ*, 842, 123
 Gárate, M., Birnstiel, T., Drązkowska, J., & Stammmer, S. M. 2020, *A&A*, 635, A149
 Gorti, U., Dullemond, C. P., & Hollenbach, D. 2009, *The Astrophysical Journal*, 705, 1237
 Guilera, O. M., Cuello, N., Montesinos, M., et al. 2019, *MNRAS*, 486, 5690
 Guilera, O. M., Miller Bertolami, M. M., & Ronco, M. P. 2017, *Monthly Notices of the Royal Astronomical Society: Letters*, 471, L16
 Haisch Jr, K. E., Lada, E. A., & Lada, C. J. 2001, *The Astrophysical Journal*, 553, L153
 Hartmann, L., Calvet, N., Gullbring, E., & D'Alessio, P. 1998, *The Astrophysical Journal*, 495, 385
 Kroupa, P. 2001, *Monthly Notices of the Royal Astronomical Society*, 322, 231
 Kunitomo, M., Ida, S., Takeuchi, T., et al. 2021, *ApJ*, 909, 109
 Kunitomo, M., Ida, S., Takeuchi, T., et al. 2021, *The Astrophysical Journal*, 909, 109
 Lynden-Bell, D. & Pringle, J. E. 1974, *MNRAS*, 168, 603
 Mamajek, E. E. 2009, in *American Institute of Physics Conference Series*, Vol. 1158, *Exoplanets and Disks: Their Formation and Diversity*, ed. T. Usuda, M. Tamura, & M. Ishii (AIP), 3–10
 Manara, C. F., Ansdell, M., Rosotti, G. P., et al. 2023, in *Astronomical Society of the Pacific Conference Series*, Vol. 534, *Protostars and Planets VII*, ed. S. Inutsuka, Y. Aikawa, T. Muto, K. Tomida, & M. Tamura, 539
 Manara, C. F., Mordasini, C., Testi, L., et al. 2019, *A&A*, 631, L2
 Manara, C. F., Rosotti, G., Testi, L., et al. 2016, *A&A*, 591, L3
 Muzerolle, J., Calvet, N., Briceño, C., Hartmann, L., & Hillenbrand, L. 2000, *The Astrophysical Journal*, 535, L47
 Natta, A., Testi, L., & Randich, S. 2006, *A&A*, 452, 245
 Owen, J. E., Clarke, C. J., & Ercolano, B. 2012, *Monthly Notices of the Royal Astronomical Society*, 422, 1880
 Pan, M., Liu, B., Jiang, L., et al. 2025, *ApJ*, 985, 7
 Pfalzner, S., Dehghani, S., & Michel, A. 2022, *The Astrophysical Journal Letters*, 939, L10
 Pfalzner, S. & Dincer, F. 2024, *ApJ*, 963, 122
 Pfalzner, S., Steinhausen, M., & Menten, K. 2014, *The Astrophysical Journal Letters*, 793, L34
 Pringle, J. E. 1981, *Annual review of astronomy and astrophysics*, 19, 137
 Ribas, Á., Bouy, H., & Merín, B. 2015, *Astronomy & Astrophysics*, 576, A52
 Ribas, Á., Espaillat, C. C., Macías, E., & Sarro, L. M. 2020, *A&A*, 642, A171
 Ribas, Á., Merín, B., Bouy, H., & Maud, L. T. 2014, *A&A*, 561, A54
 Ronco, M. P., Guilera, O. M., & de Elía, G. C. 2017, *Monthly Notices of the Royal Astronomical Society*, 471, 2753
 Ronco, M. P., Schreiber, M. R., Villaver, E., Guilera, O. M., & Miller Bertolami, M. M. 2024, *A&A*, 682, A155
 Rosotti, G. P. 2023, *New A Rev.*, 96, 101674

Appendix A: Dependence of the viscosity with the stellar mass

In order to study the impact of the parameter a in the relation $\alpha = \alpha_0 \times M_*^a$, we analyze the results of new synthetic populations adopting now $a = 1.5$ and $a = 2$. We show the cases considering the previously studied two ranges for α_0 and adopting the uniform and linear probability distribution in such ranges as in Sec. 4.2.1 and Sec. 4.2.2.

Appendix A.1: The log α_0 between -4 to -2

The Fig. A.1 and Fig. A.2 show the results for $a = 1.5$ and $a = 2$, for the uniform and linear distributions of values of α_0 , respectively. In both cases, as for the case of $a = 1.8$, the fraction of stars with discs match very well the estimations from Pfalzner et al. (2022) for the closer clusters, especially after about 5 Myr, covering disc lifetimes in the range 1 – 20 Myr in agreement with observations. Increasing the value of a generates a small reduction in the number of stars with discs at early ages. This is because for $a = 2$ stars larger than $1 M_\odot$ have discs with larger viscosities and evolve faster being the firsts to dissipate. While for $a = 2$ stars with masses below $1 M_\odot$ have discs with less viscosity, dissipation time scales become larger being dominated by the photoevaporation. Thus, both population synthesis seem very similar after about 5 Myr.

We can also see that the increment of the exponent a leads to a better correlation between accretion rates and disc and stellar masses.

Summarizing, we can observe that the distribution of $\log \alpha_0$ between -4 and -2 leads to reasonable agreement with the observation for the three values of the exponent a . This supports an observational necessity that the disc viscosity scales with the stellar mass.

Appendix A.2: The log α_0 between -3.5 to -1.5

Finally, we examine the population synthesis assuming a larger viscosity for the discs, in the range of the $\log \alpha_0$ between -3.5 and -1.5. Again, we consider both the uniform and linear distributions over the range of $\log \alpha_0$. The Fig. A.3 and the Fig. A.4 show the result for the exponent $a = 1.5$ and $a = 2.0$, respectively. As before, top raw displays the population synthesis considering the uniform distribution of the $\log \alpha_0$, while the bottom panels represent the case of the linear distribution.

As we show in Sec. 4.2.2, increasing the disc viscosities matches better the mass accretion rates as a function of the disc masses. In addition, it also matches the correlation between the mass accretion rates and the stellar masses for both values of the exponent a and for both distributions of the $\log \alpha_0$, especially the linear one.

In this sense, the population synthesis with linear distribution of $\log \alpha_0$ and the value of $a = 2$ is the one that better reproduces the fraction of stars with discs.

As we mentioned before, in the absence of external photoevaporation none of the population synthesis is able to reproduce low-mass discs with high accretion rates.

Again, the change of the correlation between disc viscosity and stellar mass seems to not play a major role, but it is necessary to reproduce the observational trend between mass accretion rates and stellar masses.

Appendix B: Variation of the dust-to-gas ratio

From the observations, the estimated masses of the discs are obtained from sub-mm continuum emission which is dominated by dust. It is known that the dust fraction in protoplanetary discs decreases over time, due to the dust radial drift and disc evolution (Sellek et al. 2019; Rosotti et al. 2019). At an age of 1.5 Myr the dust could have undergone significant radial drift and/or dust growth to larger solids, which could lead to an apparent reduction of the estimated disc gas masses. Thus, increasing the dust-to-gas ratio could lead to an increment of the dispersion on the correlation between mass accretion rates and disc masses. The Fig. B.1 show the changes in the correlation between mass accretion rates and disc gas masses considering four different gas-to-dust ratio, for our population synthesis adopting a value of $a = 1.8$, and the $\log \alpha_0$ following a linear distribution between -3.5 and -1.5. The left panel shows the $\dot{M} - M_d$ diagram for the standard dust-to-gas ratio of 1%. The consecutive panels increase this standard value of the dust-to-gas ratio in a factor 2, 3 and 4, respectively. Thus, we can see that just with a dust-to-gas ratio ratio of 4×10^{-2} we start to obtain low-mass discs with moderate and high accretion rates reproducing better the observations. This leads to the possibility that even in the absence of external photoevaporation, the correlation between the observed accretion rates and the estimated disc masses can be reproduced incorporating a dispersion in the dust-to-gas ratio for the inference of the disc masses.

Appendix C: Time evolution of the correlation between accretion rates and stellar masses

The correlation between accretion rates and stellar masses seems to represent a strong observational trend. In this appendix, we want to analyze the time evolution of our synthetic correlation. Thus, for the population synthesis described in Sec. 4.2.2 (the one adopting a linear distribution for the $\log \alpha_0$ between -3.5 and -1.5) we compute the $\dot{M} - M_*$ correlation at different times of the synthesis evolution (in the Sec. 4.2.2 such correlation was computed at 1.5 Myr of the synthesis evolution). Thus, the panels from left to right represent the synthetic correlation $\dot{M} - M_*$ at 1 Myr, 2 Myr, 3 Myr and 4 Myr, respectively, of the synthesis evolution. It is clear that as time advances, more discs dissipate. However, the synthetic correlation $\dot{M} - M_*$ seems to keep a good match with the observed correlation even at 4 Myr of evolution. This results suggest the possibility that the observed correlation between accretion rates and stellar masses presents some kind of time invariance. This could be the reason for what young stellar clusters, not all of the same age, present this observational trend. In addition, this result also supports the choice to compute synthetic accretion rates at 1.5 Myr as a representative time for young stellar cluster.

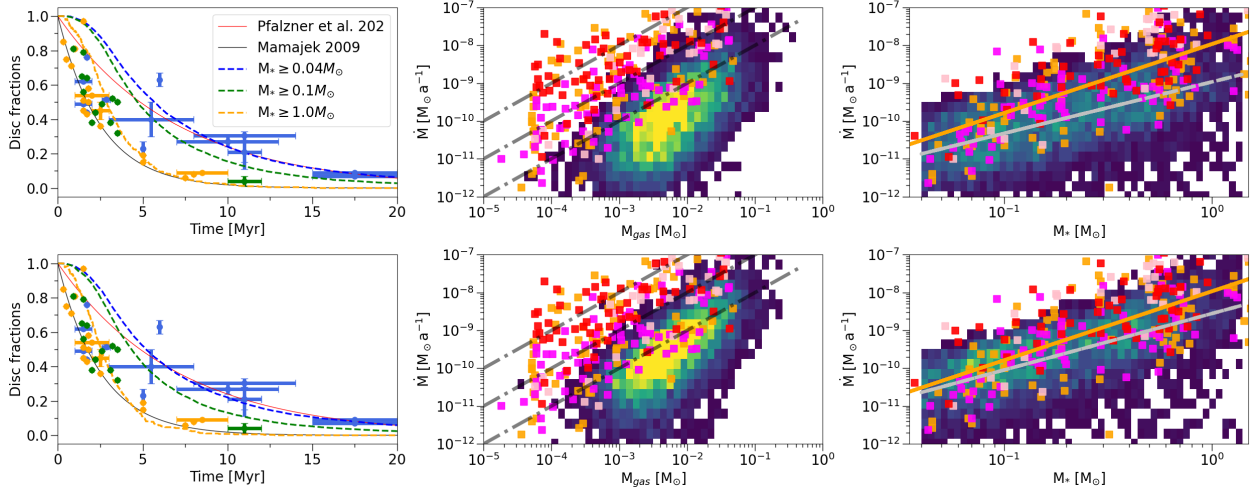


Fig. A.1. Same as Fig. 5 but adopting a value of $a = 1.5$ in the relation $\alpha = \alpha_0 \times M_*^a$.

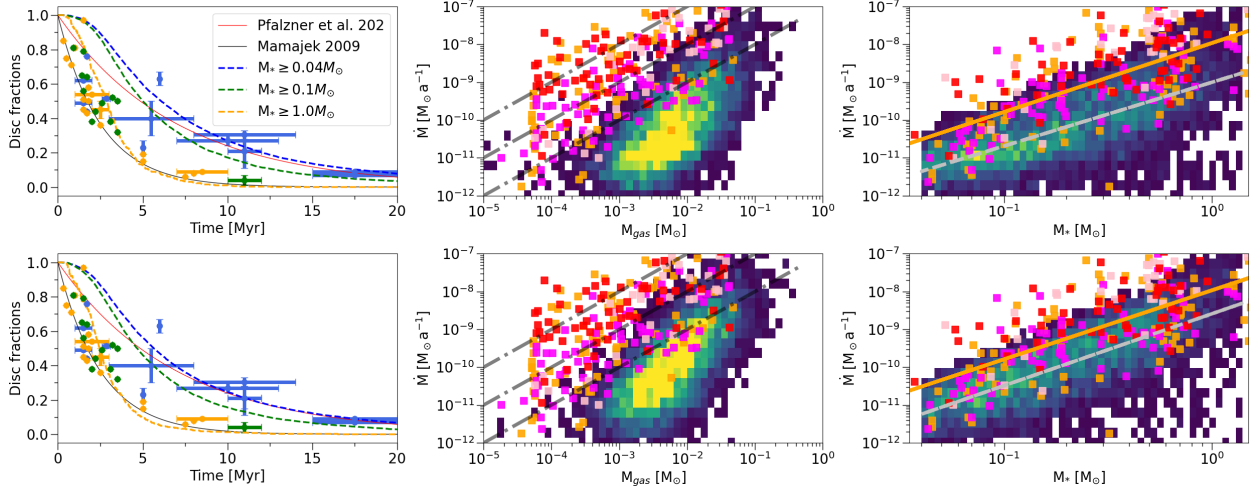


Fig. A.2. Same as Fig. 5 but adopting a value of $a = 2$ in the relation $\alpha = \alpha_0 \times M_*^a$.

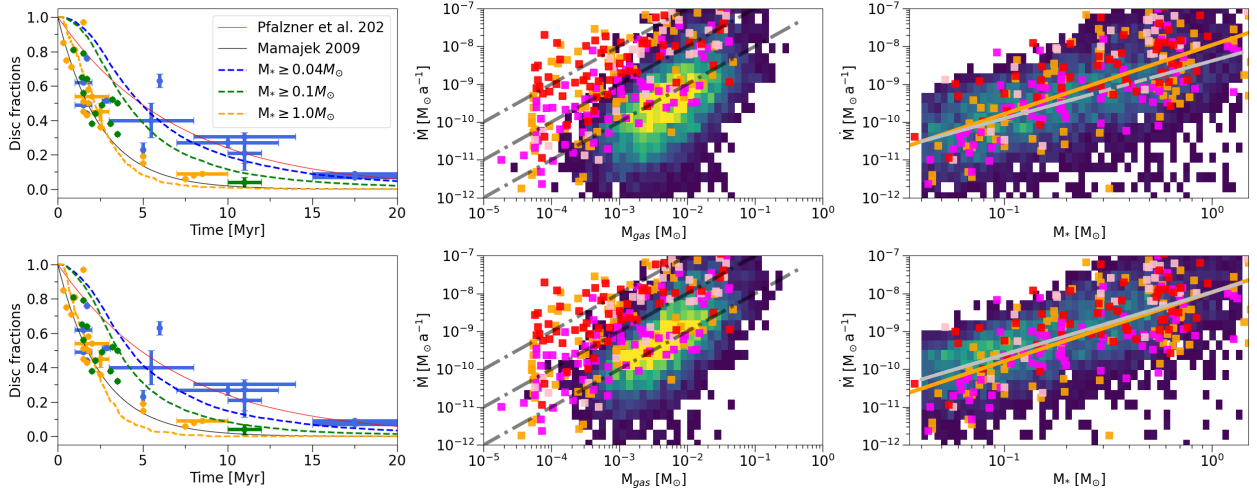


Fig. A.3. Same as Fig. 6 but adopting a value of $a = 1.5$ in the relation $\alpha = \alpha_0 \times M_*^a$.

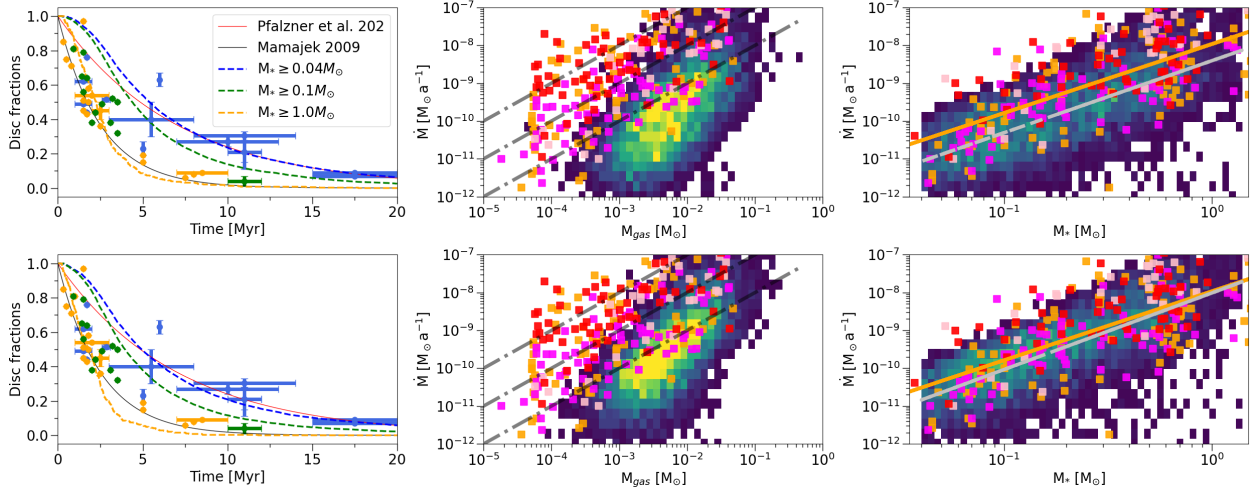


Fig. A.4. Same as Fig. 6 but adopting a value of $a = 2$ in the relation $\alpha = \alpha_0 \times M_*^a$.

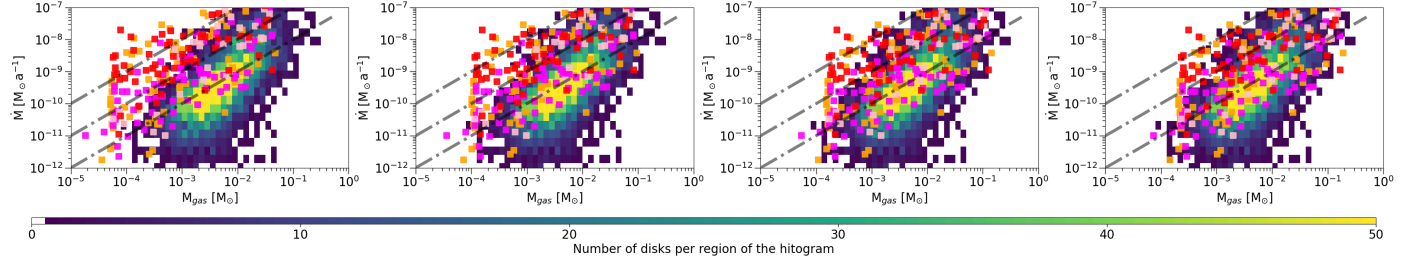


Fig. B.1. $\dot{M} - M_d$ diagrams for the population synthesis adopting a value of $a = 1.8$, the $\log \alpha_0$ following a lineal distribution between -3.5 and -1.5, and considering different dust-to-gas ratios to compute the disc masses. The panels from left to right represent the population synthesis adopting a dust-to-gas ratio of 10^{-2} , 2×10^{-2} , 3×10^{-2} and 4×10^{-2} , respectively.

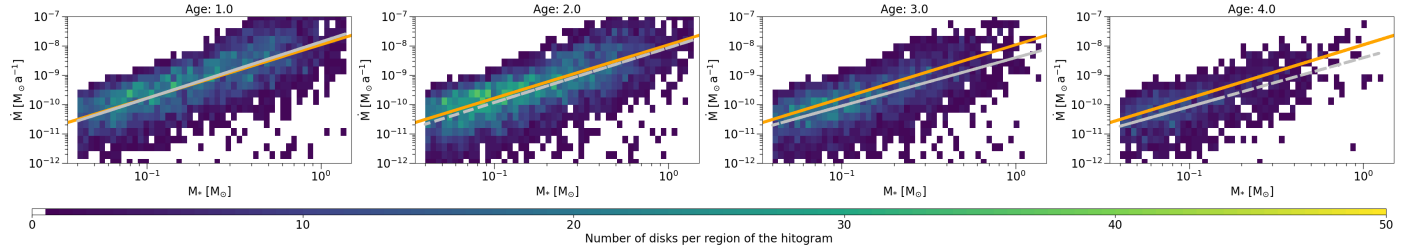


Fig. C.1. Time evolution of the diagram $\dot{M} - M_*$ for the population synthesis used in Sec. 4.2.2, i. e. considering $a = 1.8$, the $\log \alpha_0$ following a lineal distribution in the range between -3.5 and -1.5, and a SFR with $t_d = 1$ Myr.